Diapycnal Mixing in a Conceptual Model of the Atlantic Meridional Overturning Circulation

Ben Marzeion *, Helge Drange

Nansen Environmental and Remote Sensing Center & Bjerknes Center for Climate Research, Thormøhlensgate 47, N-5006 Bergen, Norway

Abstract

A three-box model of the Atlantic Ocean is used to examine the influence different parameterisations of the diapycnal mixing may have on the large scale dynamics of the ocean circulation. Special emphasis is given to the northward volume and heat transports. The vertical diffusivity κ is taken in the general form $\kappa \sim N^{-\alpha}$, where N is the buoyancy frequency, and the parameter space $0 \leq \alpha \leq 3$ is explored. An imposed freshwater forcing of the northern high latitude box is used as a test case to investigate the behaviour of the model compared to similar types of sensitivity experiments carried out with, for instance, General Circulation Models. Four different solution states are identified, separated by three critical values of α. For small values of α, both heat and volume fluxes decrease with increasing freshwater flux. Increasing α leads first into a parameter domain where the transport of heat increases with increasing freshwater forcing, then at even higher α also the volume transport increases. Finally, a fourth state is found where strong advection of warm water leads to an increase of the northern box temperature, as opposed to cooling for small α. The behaviour of the critical values of α is discussed with respect to model dynamics and parameters. A subtle interplay between changes in the thermocline depth and the advective fluxes from the thermocline box into northern box, which both are modulated by diapycnal mixing, is found to be the key process in determining the behaviour of the model. Finally, the implications for modelling and understanding of basic features of the ocean circulation are discussed.

Key words: Meridional oceanic circulation, Modelling, Vertical mixing, Thermocline
PACS: 92.10.Mr, 92.10.Lq

* corresponding author
Email address: ben.marzeion@nersc.no (Ben Marzeion).

1 Introduction

A considerable fraction of the climate system's northward heat transport is provided by the Atlantic Ocean Meridional Overturning Circulation (MOC). The strength and variability of the Atlantic MOC are therefore important factors for the climate of the North Atlantic region. Simulations of future climate scenarios using climate General Circulation Models (GCMs) suggest that under increased greenhouse gas forcing, the freshwater flux into the North Atlantic ocean will increase as a result of an intensified hydrological cycle as well as a gradual melting of the cryosphere. Since an anomalous strong input of freshwater to high latitudes will increase the vertical stability of the water column, the deep water formation rate might reduce or even cease. This in turn might lead to a decrease of the overturning, causing a cooling of the North Atlantic region (e.g. Manabe and Stouffer, 1993; Schmittner and Stocker, 1999).

A similar mechanism has been proposed to explain features of past climate variability, as when the Earth underwent large and rapid climate changes during the last glacial and postglacial periods. The origin of the abrupt changes is heavily discussed, but a number of studies suggest that the Atlantic MOC played an active and important role in these rapid transitions (e.g. Rahmstorf, 1995; Broecker, 1997; Ganopolski and Rahmstorf, 2001; Rahmstorf, 2002; McManus et al., 2004).

However, based on the findings of Sandström (1908), it has been argued that it is rather the downward mixing of heat at low latitudes that limits the sustainable rate of overturning in the sense of energy input. Recently, this argument was strengthened by Munk and Wunsch (1998), Marotzke and Scott (1999) and Huang (1999) by means of theoretical considerations and idealised model studies. It has also been proposed that the Southern Ocean, through northward-directed Ekman pumping of the thermoclime waters and subsequent mixing, is an important factor for the variability and stability of the Atlantic MOC (e.g. Toggweiler and Samuels, 1995; Knorr and Lohmann, 2003).

It is thus important to gain understanding in how the representation of mixing processes influences a model's behaviour, as well as to identify possible responses of the overturning to perturbations in the light of a circulation driven by mixing.

The common way to embed unresolved processes in ocean GCMs is to mimic the effect of the sub-grid scale processes by certain empirically and theoretically-based rules or parameterisations from the explicitly modelled local or large-scale dynamics. The diapycnal, or vertical, mixing in ocean GCMs is, in gen-

eral, not explicitly modelled, but prescribed or parameterised. At least four classes of vertical mixing schemes can be identified: 1) The mixing is constant in time and space, 2) the mixing is constant in time but varying in space; 3) the mixing is deduced from, in general, simple dependencies or combinations of local or large-scale prognostic variables, and 4) the mixing is determined by explicit, or prognostic, modelling of the actual physical processes governing the mixing. Obviously, class 3) and 4) lead to mixing that vary in time and space. The majority of ocean GCMs and climate GCMs belongs to class 1) or 2). A few ocean GCMs and climate GCMs fall into class 3), notably the isopycnic co-ordinate ocean GCMs that commonly uses the dependency $\kappa \sim N^{-\alpha}$. Here κ is the vertical diffusivity, N is the buoyancy frequency and α is a dimensionless parameter, the latter often chosen close to unity (e.g. Bleck et al., 1992; Otterå et al., 2003).

The effect of freshwater forcing and the strength of the vertical mixing on the stability of MOC has been studied using climate GCMs (Manabe and Stouffer, 1999), ocean GCMs (e.g. Park and Brian, 2000; Klinger et al., 2003; Prange et al., 2003) and box models (e.g. Tziperman et al., 1994; Griffies and Tziperman, 1995; Park, 1999). However, none of these studies did explicitly explore the models' sensitivity to a density stratification dependent vertical mixing coefficient.

Nilsson and Walin (2001) used a two-layer model for the northern hemisphere, employing three different parameterisations of the diapycnal mixing. This way they were able to identify two different regimes of the overturning circulation: The classical, well-known regime where the overturning decreases with increased freshwater flux when the diffusivity was independent of the stratification; and a regime where the overturning was enhanced by increased freshwater forcing when the mixing was a function of the stratification. This means that Stommel's salinity feedback (Stommel, 1961) changes sign from positive to negative.

Mohammad and Nilsson (2004) and Nilsson et al. (2003) extended the Nilsson and Walin (2001) study using a 2-dimensional numerical model and showed that for a critical value of the freshwater forcing, the model would either produce strong oscillations (in the case of stratification dependent mixing), or the well-known reversed, haline-driven flow with sinking in the south (in the case of constant diffusivity). Oliver et al. (2005) used a time-dependent 3-box model to show that the negative salinity feedback caused by limited mixing is only valid in a small parameter domain. The reason for this is that the timescale of the advective-diffusive adjustment of the thermocline is longer than the time required to change the overturning.

In this study, we address the question of how different mixing regimes influence the behaviour of quantities important to the climate system, such as

the oceanic heat transport. We use a time-dependent, three-box model of the thermocline based on the model proposed by Gnanadesikan (1999), thus similar to the models used by Nilsson and Walin (2001) and Oliver et al. (2005), but incorporating the southern hemisphere. Based on the common assumption that stratification limits the rate at which heat is mixed downward, a general parametrisation for the diapycnal mixing is proposed as $\kappa \sim N^{-\alpha}$. It is then shown that the relation between freshwater forcing, volume and heat transports varies considerably over the range $0 \leq \alpha \leq 3$.

Contrary to the common perception and additionally to what has been shown by Nilsson et al. (2003), Oliver et al. (2005) and Mohammad and Nilsson (2004), we find that the anomaly of the northward transport of heat due to changes in the freshwater forcing changes sign for much weaker dependency of mixing on stratification (i.e. smaller α) than the volume flux anomaly does. Furthermore, if the dependency of the mixing on stratification is particularly strong, also the temperature anomaly in the northern box may change sign. This leads to the counter-intuitive finding of warming as response to an increased freshwater flux.

In section 2 we discuss the model and experiments used for this study. The results are presented in section 3. Finally, both implications and limitations of this analyses are addressed in section 4.

2 Model

A schematic representation of the model is given in fig. 1. There is one shallow box representing the low to mid latitude thermocline waters. A second box represents the northern North Atlantic and the deep water underlying the thermocline. Finally, the third box represents the water of the Southern Ocean. To reflect the measures of the Atlantic Ocean, the total water depth D is set to 4000 m, the width B is set to 5000 km, and the length L is set to 12000 km, of which the thermocline box occupies $1/2$ L, and each of the northern and southern boxes $1/4$ L.

2.1 Horizontal fluxes between the boxes

The dynamic equations are based on the model by Gnanadesikan (1999), with two major differences: First, the volume fluxes are not assumed to balance at all times, but the volume of the thermocline box may vary on cost of the northern, deep box. Second, density differences between the boxes are not prescribed, but modelled, and thus include advective feedbacks.

The conservation of volume then takes the time dependent form

$$A\frac{dH}{dt} = \Psi_{\mathrm{Up}} - \Psi_{\mathrm{Ed}} + \Psi_{\mathrm{Ek}} - \Psi_{\mathrm{No}} \tag{1}$$

where A is the horizontal area of the thermocline box, and H is the thickness scale of the thermocline depth. Diapycnal upwelling Ψ_{Up} is calculated from the advective-diffusive balance as

$$\Psi_{\mathrm{Up}} = \frac{A\kappa}{H} \tag{2}$$

with κ the diapycnal diffusivity. Ψ_{Ed} is the eddy-induced transport, which is represented by the parameterisation (Gent and McWilliams, 1990; Gent et al., 1995):

$$\Psi_{\mathrm{Ed}} = \frac{BA_iH}{L_y} \tag{3}$$

with B the width of the basin, A_i the eddy diffusion coefficient, and L_y the width over which the gradient in thermocline thickness is assumed to occur. The wind-driven Ekman flux into the thermocline Ψ_{Ek} is calculated as

$$\Psi_{\mathrm{Ek}} = \frac{B\tau}{f\rho_0} \tag{4}$$

with τ the typical wind stress at Drake Passage latitudes, f the Coriolis parameter, and ρ_0 a reference density. The northward volume flux Ψ_{No} is calculated as the transport of a frictional boundary current,

$$\Psi_{\mathrm{No}} = C\frac{g\Delta\rho H^2}{\rho_0\beta L_y} \tag{5}$$

where g is gravity acceleration, $\Delta\rho$ is the density difference between the northern and thermocline boxes, and β is the meridional derivation of the Coriolis parameter. The constant C incorporates effects of the boundary layer structure.

For most of the experiments shown here, a standard parameter set was used. The values for the model parameters are listed in table 1. Using these standard values, the model at steady state has an overturning of $\Psi_{\mathrm{No}} \sim 18$ Sv, with Ψ_{Up} contributing ~ 14 Sv, $\Psi_{\mathrm{Ek}} \sim 5$ Sv, and $\Psi_{\mathrm{Ed}} \sim 1$ Sv. Furthermore, the thermocline depth H is ~ 260 m, and the density difference $\Delta\rho$ is ~ 1.6 kg/m^3. For a detailed discussion of the model and parameters see Gnanadesikan (1999).

Temperature evolves according to the equations

$$\frac{d}{dt}\begin{pmatrix} T_n \\ T_e \\ T_s \end{pmatrix} = -\begin{pmatrix} u_{\mathrm{No}}\left(\frac{T_n - T_e}{L/2}\right) \\ u_{\mathrm{Ek}}\left(\frac{T_e - T_s}{L/2}\right) \\ u_d\left(\frac{T_s - T_n}{L}\right) \end{pmatrix} - \begin{pmatrix} 0 \\ u_{\mathrm{Up}}\left(\frac{T_e - T_n}{H}\right) \\ u_{\mathrm{Ed}}\left(\frac{T_s - T_e}{L/2}\right) \end{pmatrix} + \begin{pmatrix} (T_{n_{\mathrm{relax}}} - T_n)/\gamma_n \\ (T_{e_{\mathrm{relax}}} - T_e)/\gamma_e \\ (T_{s_{\mathrm{relax}}} - T_s)/\gamma_s \end{pmatrix} \quad (6)$$

where the velocities u_{No}, u_{Ek}, u_{Ed}, and u_{Up} are calculated from the net volume fluxes with respect to the crossection of the interface between the two boxes. The deep flow u_d from the northern into the southern box is calculated as the residual of Ψ_{Ed} and Ψ_{Ek}. With the parameters used for the model runs presented here, $\Psi_{\mathrm{Ek}} > \Psi_{\mathrm{Ed}}$, implying that the deep flow from the northern into the southern box is southward at all times.

The heat fluxes are specified through relaxation to prescribed temperatures ($T_{n_{\mathrm{relax}}}$, $T_{e_{\mathrm{relax}}}$, and $T_{s_{\mathrm{relax}}}$). The role of the different relaxation timescales γ_n, γ_e, and γ_s is discussed in section 3.

The evolution of salinity assumes a similar form:

$$\frac{d}{dt}\begin{pmatrix} S_n \\ S_e \\ S_s \end{pmatrix} = -\begin{pmatrix} u_{\mathrm{No}}\left(\frac{S_n - S_e}{L/2}\right) \\ u_{\mathrm{Ek}}\left(\frac{S_e - S_s}{L/2}\right) \\ u_d\left(\frac{S_s - S_n}{L}\right) \end{pmatrix} - \begin{pmatrix} 0 \\ u_{\mathrm{Up}}\left(\frac{S_e - S_n}{H}\right) \\ u_{\mathrm{Ed}}\left(\frac{S_s - S_e}{L/2}\right) \end{pmatrix} + \begin{pmatrix} Q_n^{\mathrm{salt}} \\ Q_e^{\mathrm{salt}} \\ (S_{s_{\mathrm{relax}}} - S_s)/\gamma_s^S \end{pmatrix} \quad (7)$$

where Q_n^{salt} and Q_e^{salt} are virtual salt fluxes corresponding to prescribed freshwater fluxes F_n and F_e, respectively. The southern salinity is relaxed to a constant value $S_{s_{\mathrm{relax}}}$ to mimic the effect of the Antarctic Circumpolar Current.

An equation of state both linear in temperature and salinity is employed to calculate the density within each of the boxes.

2.2 Diapycnal Diffusivity

Diapycnal mixing is believed to be strongly influenced by stratification, since more turbulent kinetic energy is needed to displace water over a strong vertical density gradient. We hypothesise that the relation between diffusivity κ and the stratification, measured by the buoyancy frequency N, can be expressed as

$$\kappa = c\left(\frac{N}{N_0}\right)^{-\alpha} \quad (8)$$

where $c = 9{\cdot}10^{-5}$ m^2 s^{-1} is a constant, $N_0 = 8{\cdot}10^{-3}$ s^{-1} is a reference buoyancy freqency, and N is calculated as

$$N^2 = -\frac{g\Delta\rho}{\rho_0 H}$$

with $\Delta\rho$ the density difference between the northern and thermocline boxes. Thus, both changes in thermocline depth and density difference are accounted for in equation 8. However, since changes in H are relatively small ($\sim$ 15 m, see figure 2) in all the experiments presented here, changes of the value of κ generally reflect changes in $\Delta\rho$.

Equation 8 is similar to the relation between the dissipation of turbulent kinetic energy per mass ε and the stratification N as suggested by Gregg (1989) and Gargett and Holloway (1984), that is

$$\varepsilon \sim N^m$$

with $1 \leq m \leq 2$.
Using the relation

$$\kappa \sim \varepsilon / N^2$$

this corresponds to $0 \leq \alpha \leq 1$. However, Rehmann and Duda (2000) find $\alpha = 3.1$ close to the bottom of a shelf slope, and $\alpha = 1.3 \pm 0.8$ to be representative for the whole water column. Also, Fer et al. (2004) find $\alpha = 1.2 \pm 0.5$ in an Arctic fjord, suggesting that the value of α might in fact not be limited by 0 and 1. Furthermore, vertical profiles of the tracers ^{222}Rn and ^{228}Rn in the deep ocean (Sarmiento et al., 1976), penetration of bomb-produced tritium into the pycnocline of the Norwegian Sea (Hoffert and Broecker, 1978; Broecker and Peng, 1982, Chap. 7), and spreading of radioactive material from a dumpsite (OECD, 1985), indicate that $\kappa \sim N^{-2}$.

In this study, we therefore take the general approach as in equation 8, and let α vary between 0 and 3. The experiments with α close to 3 is mainly included for illustrative purposes.

At steady state, this means that the upwelling Ψ_{Up} scales with the density difference $\Delta\rho$ between the northern and low latitude boxes like (from equation 2)

$$\Psi_{\mathrm{Up}} \sim \Delta\rho^{-\frac{\alpha}{2}} H^{\frac{\alpha}{2}-1}$$

Note, however, that via the advection and volume continuity a feedback between Ψ_{Up}, H and $\Delta\rho$ exists so that neither of the variables can be derived directly as a function of e.g. the freshwater forcing F_n.

2.3 Experiments

A large number of simulations are performed where the parameter α is varied systematically between 0 and 3. At the same time, the freshwater forcing is varied between 50% and 150% of the default value 0.24 Sv (this is equivalent to 0.5 m yr^{-1}), representing the present climate.

With this setup, it is possible to identify four different dynamic regimes. To investigate the processes that are characteristic for each regime, single model runs are made for exemplary values of α. In these constructed realisations, the northern freshwater forcing F_n is increased by 50% after the model has come to a steady state.

Finally, the southern ocean wind stress τ, and the timescale γ_n used for temperature adjustment of the northern box are varied to test the robustness of the results and the influence that southern ocean processes may have on the behaviour of the North Atlantic.

3 Results

Table 2 provides an overview over the properties of the four regimes that are presented in detail in the following sections.

3.1 Decreasing heat and volume transports ($\alpha < \alpha_{\mathrm{heat}}$)

Figure 4 shows the anomalous net transport of heat Q_n^{ocean} into the northern box when the model is at steady state. It is calculated as the divergence of the heat flux in the northern box as

$$Q_n^{\mathrm{ocean}} = \rho_0 c_p (T_e - T_n)\Psi_{\mathrm{No}}$$

where c_p is the specific heat capacity of seawater, and can thus be interpreted as the amount of heat released into the overlying atmosphere. For increasing freshwater forcing, the net heat transport decreases for $\alpha < 0.14 \stackrel{\mathrm{def}}{=} \alpha_{\mathrm{heat}}$ (the

critical values of α for this and the following regimes are approximations taken at the default freshwater forcing of 0.24 Sv).

Figure 3 shows the same plot, but for the anomaly of the northward volume transport Ψ_{No}, which decreases with increasing freshwater forcing for $\alpha < 0.71 \stackrel{\mathrm{def}}{=} \alpha_{\mathrm{psi}}$. This regime represents a weak dependency of the diapycnal mixing on the stratification, and is modeled by GCMs using $\alpha = 0$.

The black lines of figs. 2, 5 and 6 correspond to this regime: Since the increased freshwater flux decreases the density difference between the thermocline and northern/deep boxes (fig. 2), the northward volume transport Ψ_{No} initially drops (fig. 5). This leads to an imbalance of the volume fluxes into and out of the thermocline box, and the thermocline depth H increases (fig. 2). Since $\Psi_{\mathrm{Up}} \sim H^{-1}$, the upwelling decreases as well, until the two fluxes balance again and the system reaches steady state. Ψ_{No} recovers slowly as it scales as H^2. The weakened advection leads to a greater temperature difference between the thermocline and northern boxes (fig. 6), but it is the strong decline in the volume flux (fig. 3) that is responsible for the decreased amount of heat transported into the northern box (fig. 4).

This regime however exists only in a very limited region of the parameter space. Figure 7 shows the dependency of α_{heat} on the timescale used for temperature relaxation of the northern box. Increasing this timescale increases the relative importance of advection for the heat budget of that box. At relaxation timescales longer than 10 years, this regime disappears.

3.2 Increasing heat, decreasing volume transports ($\alpha_{\mathrm{heat}} < \alpha < \alpha_{\mathrm{psi}}$)

For $\alpha > \alpha_{\mathrm{heat}}$, the model dynamics change character. While the transport of volume decreases by enhanced freshwater flux until $\alpha = \alpha_{\mathrm{psi}}$ (see fig. 3), the net northward heat transport is now increased (fig. 4). This happens although the increase in temperature difference is weaker (see red line in fig. 6). The reason is that for e.g. $\alpha = 0.5$, Ψ_{Up} now scales like $\Psi_{\mathrm{Up}} \sim \Delta\rho^{-1/4} H^{-3/4}$, initiating an increase of the upwelling as a response to the reduced density difference. The weakening effect of the increase in H is reduced as well, so that steady state is reached at a greater H than before (fig. 2). Because $\Psi_{\mathrm{No}} \sim H^2$, the tendency for weaker overturning is reduced. Together, this leads to an increase in the heat flux as seen in fig. 4. The upper limit of this regime is reached at α_{psi}, where the volume transport anomaly changes its sign.

3.3 Freshwater boosted regime ($\alpha_{\text{psi}} < \alpha < \alpha_{T_{\text{no}}}$)

The "freshwater-boosted" regime has previously been described by e.g. Nilsson and Walin (2001) and Nilsson et al. (2003). It arises when the change in Ψ_{No} is governed by H, rather then by $\Delta\rho$. In the model presented here, this is the case when $\alpha > \alpha_{\text{psi}}$ (see fig. 3). For the case $\alpha = 1$ (blue line in figs. 2, 5 and 6), the uppwelling now scales like $\Psi_{\text{Up}} \sim \Delta\rho^{-1/2}H^{-1/2}$. As before, the northward transport Ψ_{No} initially decreases in response to the weakened density difference. At the same time, the increase of Ψ_{Up} starts to fill the thermocline (figs. 2 and 5). The resulting increase in H leads to the recovery and overcompensation of Ψ_{No}. Since the increase in transport is caused by a greater cross-section area rather then larger velocity, advection of heat is still weakened, leading to an increase of the temperature gradient (fig. 6). Together with the increased volume transport, this supports a strengthening of the northward heatflux as seen in fig. 4.

Figure 7 shows that the critical value α_{psi} increases with the timescale of the northern temperature relaxation. Increasing the relaxation timescales weakens the temperature difference by advection, implying a reduced density difference. As is discussed above, because $\Psi_{\text{Up}} \sim \Delta\rho^{-1/2}H^{-1/2}$ this in turn tends to increase the thermocline depth H. The relative influence of the increase of Ψ_{Up} on H is thus weaker, causing α_{psi} to increase.

3.4 Advection dominated regime ($\alpha > \alpha_{T_{\text{no}}}$)

The advective northward velocity u_n depends linearly on the thermocline depth H and the density difference $\Delta\rho$. As discussed above, the response of H to freshwater forcing increases with α. Thus, with increasing α the advective term in the heat budget of the northern box becomes more important. As the critical value $\alpha_{T_{\text{no}}} \approx 2.16$ is reached (see fig. 8), the temperature response of the northern box is reversed. In fig. 6 one can see that at $\alpha = 3$, the temperature difference is decreased as a response to the freshwater pulse. This acts as a positive feedback, further reducing the density difference. This feedback is weakened by advection of salt, which works the same way, but acts as a negative feedback. However, since haline contraction play a lesser role than thermal expansion, advection always acts as a positive feedback in a model with a linear equation of state.

The timescale γ for the temperature relaxation of the northern box determines the relative importance of surface heat fluxes and advective processes in the box. As can be seen in fig. 7, increasing γ therefore leads to decreasing $\alpha_{T_{\text{no}}}$.

Generally speaking, the two volume fluxes Ψ_{Ek} and Ψ_{Ed}, representing the southern ocean processes, act to fill or empty the thermocline box, thereby changing H. However, in contrast to changes in the thermocline volume caused by the northern freshwater flux as discussed above, this happens without influencing the thermohaline properties of the northward and upwelling flows. We use the wind stress as an example on how these southern ocean processes influence the properties of the northward flow while leaving A_i constant, and discuss the relevance this has for the results found above.

In fig. 9, the critical values of α are plotted against the magnitude of the southern wind stress forcing. The red line marks the value of α where the heat transport anomaly changes from negative to positive sign. By increasing the southern wind stress, more water from the southern ocean is pumped into the thermocline. As a result, the thermocline deepens towards steady state. At the same time, increasing the freshwater flux also increases thermocline depth. At stronger wind forcing, however, the relative increase is weaker. While the effect of the freshwater flux on the temperature difference remains the same, the influence on the volume transport is weakened. This results in a smaller value of α_{heat}.

The effect of wind stress on the northward volume flux is similar to increasing the relaxation timescale for the temperature forcing: Both act to increase thermocline depth, however, the wind stress does so without reducing the temperature difference. The diminishing effect of τ on α_{psi} is therefore weak, and can be considered negligible in the setting of a box model as simple as the one presented here.

For $\alpha_{T_{\mathrm{no}}}$, the mechanism is similar: Increasing the initial thermocline depth causes a relative weakening of the increase in H caused by the freshwater flux, which tends to increase advection. Therefore, α must be increased to cause a warming in the northern box if the southern wind stress is increased.

4 Discussion

A major challenge in the development of ocean GCMs is linked to the fact that for real applications, the ocean GCMs are restricted to be run with a spatial resolution that is far too coarse to explicitly resolve small-scale processes. There are many examples that unresolved processes (e.g., tidally driven mixing, mixing over rough topography, breaking of internal waves, convective mixing) may feed back to, and alter, the large-scale dynamics of the system

(e.g. Munk and Wunsch, 1998; Hasumi and Suighinohara, 1999; Kim and Stössel, 2001; Jayne and St. Laurent, 2001; Kim et al., 2003; Harper et al., 2004; Simmons et al., 2004), illustrating the importance of sub-grid scale parameterisations.

There are furthermore many examples that the strength of the MOC critically depends on the magnitude or the vertical profile of the diapycnal or vertical mixing (e.g. Bryan, 1987; Cummins et al., 1990; Manabe and Stouffer, 1999; Gao et al., 2003). Additionally, Manabe and Stouffer (1999) demonstrated that the overturning circulation in ocean GCMs forced with a time-limited surface fresh water anomaly is prone to run into an irreversible collapse (an Atlantic MOC in "off" mode) for weak vertical mixing, whereas strong vertical mixing lead to a recovery of the MOC ("on" mode) after the anomalous fresh water forcing was switched off. The latter finding is consistent with the results of Schiller et al. (1997), using a model system quite different from that of Manabe and Stouffer (1999), indicating robustness of the obtained results. Furthermore, Cummins et al. (1990) showed that it is possible to tune the strength of the MOC without affecting the poleward heat transport by varying the magnitude of the vertical mixing with depth.

The intrinsic stability properties of MOC in a fresh-water forced ocean system have received considerable attention recently (e.g. Nilsson and Walin, 2001; Nilsson et al., 2003; Prange et al., 2003; Mohammad and Nilsson, 2004; Oliver et al., 2005). All of these studies have confirmed the findings of Manabe and Stouffer (1999) that the MOC depends on the formulation (or magnitude) of the vertical mixing. In fact, e.g. Nilsson and Walin (2001) and Nilsson et al. (2003) show, contrary to the general belief, that the thermohaline circulation may increase as a result of increased fresh water forcing. The latter result was obtained for $\kappa \sim N^{-1}$. It can here be mentioned that in a climate GCM with $\kappa \sim N^{-1}$, the Atlantic MOC started to recover after about 50 years integration despite a continuous 150 years supply of fresh water to the high northern latitudes (e.g. Otterå et al., 2003, 2004).

The presented analyses, based on a three-box model formulated by scaling of the governing equations used in ocean GCMs (Gnanadesikan, 1999), indicate that a fresh water perturbed Atlantic MOC may exhibit four characteristic regimes if the vertical (or diapycnal) mixing κ is parameterised as $\kappa \sim N^{-\alpha}$. For small values of α (i.e., for $\alpha \approx 0$), both heat and volume fluxes decrease with increasing freshwater flux. This solution regime represents the classical scaling of Bryan (1987). Increasing α leads to a solution regime where the volume transport decreases but the transport of heat increases with increasing freshwater forcing. For the applied model system, this regime is bounded by $0.14 < \alpha < 0.71$. For $\alpha \approx 1$, also the volume transport increases. The latter regime, with opposite salinity feedback of the Stommel (1961) model, has been described as the freshwater boosted regime by Nilsson and Walin (2001) and

Nilsson et al. (2003). Finally, a fourth state is found for $\alpha > 2.2$ where strong advection of warm water leads to an increase of the northern box temperature, as opposed to cooling for smaller α.

While our model retains some of the features of the conceptual model of Gnanadesikan (1999), in particular the scaling $\Psi_{\mathrm{No}} \sim H^2$, the approach to model $\Delta\rho$ instead of prescribing it changes the model's behaviour significantly. Most important, changes in H as a response to changes in $\Delta\rho$ are very small (fig. 2). Using a coupled climate model, Levermann and Griesel (2004) were also unable to reproduce the large variations in pycnocline depth found by Gnanadesikan (1999). In our model, this leads to a rather weak sensitivity of the overturning strength to freshwater forcing. However, it should be noted that the main conclusions of our study do not depend on the absolute values of changes in H, but on the relative influence of the parameterization of κ.

Saenko and Weaver (2003) emphasize the role of Southern Ocean eddies for balancing changes in the northward volume transport, which are introduced by a fixed mixing energy paramerterization of the vertical diffusivity. As in their study, the deepening of the thermocline in our model is weakened by an enhanced eddy flux. However, since our model dimensions are chosen to represent the Atlantic Ocean (as opposed to a basin representing the global ocean in their study), the width over which the eddy fluxes are increased is smaller, and the influence of Southern Ocean processes is weaker.

The strength of the presented analysis is that a simple and highly idealised model formulation enables us to diagnose the characteristic behaviour of a complex system like the freshwater forced Atlantic MOC. The underlying processes and feedbacks can be explored in detail, which is a difficult task based on the output from ocean GCMs or climate GCMs.

The weakness of the presented analyses is also linked to the simplicity of the model formulation. The four identified solution regimes need to be verified by ocean GCMs to confirm the obtained results. Existing simulations and analyses (e.g. Gnanadesikan, 1999; Manabe and Stouffer, 1999; Nilsson and Walin, 2001; Nilsson et al., 2003; Oliver et al., 2005; Otterå et al., 2004; Mohammad and Nilsson, 2004) suggest that parameter regime one and three, i.e., α near zero and unity, are present in ocean GCMs. This gives credibility to the model formulation used here. Parameter regimes two ($0.14 < \alpha < 0.71$) and four ($\alpha > 2.2$) remain to be identified in ocean GCMs.

Some cautionary comments should be mentioned: Although the presented model is time dependent, the timescales may not be realistic. Since the deep water underlying the thermocline and the region of deep water formation are contained within a single box, any perturbations at the surface are instantaneously communicated to the deep interior. Since the deep water properties are

in fact set at the surface where the deep water is formed, this is not a problem when discussing steady state. On short timescales however, the actual sinking of water may be limited by stratification. The fact that this possibility is not resolved may explain the relative insensitivity of the circulation to freshwater forcing compared to studies using GCMs (see e.g. Vellinga et al., 2002; Otterå et al., 2004). Furthermore, the dependency of critical values of α on the temperature boundary conditions (fig. 7) illustrates the limitations of an uncoupled model formulation and suggests that coupling of a simple atmosphere model might be enlightening.

In summary, it has been demonstrated that depending on the parameterization of the diapycnal mixing, the response of a freshwater forced Atlantic Ocean may exhibit four different solution regimes. The boundaries of these regimes depend on a subtle interplay between processes involving the overturning of the model. Advective feedbacks and changes in thermocline depth are identified as the key processes to characterize the different solution regimes.

Acknowledgements

We thank Ingo Bethke for valuable discussions on model setup and results. We thank A. Levermann and K. I. C. Oliver for many thoughtful comments that improved the manuscript significantly. The work is a part of the *NOClim 2* project under the *Research Council of Norway*. This is publication nr. A102 of the Bjerknes Centre for Climate Research.

References

Bleck, R., Rooth, C., Hu, D., Smith, L. T., 1992. Salinity-driven Thermocline Transients in an Wind- and Thermohaline-forced Isopycnic Model of the North Atlantic. Journal of Physical Oceanography 22, 1486–1505.

Broecker, W. S., 1997. Thermohaline Circulation, the Achilles Heel of Our Climate System: Will Man-Made CO_2 Upset the Current Balance? Science 278, 1582–1588.

Broecker, W. S., Peng, T., 1982. Tracers in the Sea. Lamont-Doherty Geological Observatory, Palisades, N. Y.

Bryan, F., 1987. Parameter Sensitivity of Primitive Equation Ocean General Circulation Models. Journal of Physical Oceanography 17, 970–986.

Cummins, P. F., Holloway, G., Gargett, A. E., 1990. Sensitivity of the GFDL ocean general circulation model to a parameterisation of vertical diffusion. Journal of Physical Oceanography 20, 817–830.

Fer, I., Skogseth, R., Haugan, P. M., 2004. Mixing of the Storfjorden overflow

(Svalbard Archipelago) inferred from density overturns. Journal of Geophysical Research 109, doi:10.1029/2003JC001968.

Ganopolski, A., Rahmstorf, S., 2001. Rapid changes of glacial climate simulated in a coupled climate model. Nature 409, 153–158.

Gao, Y., Drange, H., Bentsen, M., 2003. Effects of diapycnal and isopycnal mixing on the ventilation of CFCs in the North Atlantic in an isopycnic coordinate OGCM. Tellus B 55, 837–854.

Gargett, A. E., Holloway, G., 1984. Dissipation and diffusion by internal wave breaking. Journal of Marine Research 42, 15–27.

Gent, P. R., McWilliams, J. C., 1990. Isopycnal Mixing in Ocean Circulation Models. Journal of Physical Oceanography 20, 150–155.

Gent, P. R., Willebrand, J., McDougall, T. J., McWilliams, J. C., 1995. Parameterizing Eddy-induced Tracer Transports in Ocean Circulation Models. Journal of Physical Oceanography 25, 463–474.

Gnanadesikan, A., 1999. A Simple Predictive Model for the Structure of the Oceanic Pycnocline. Science 283, 2077–2079.

Gregg, M. C., 1989. Scaling turbulent dissipation in the thermocline. Journal of Geophysical Research 94, 9686–9698.

Griffies, S. M., Tziperman, E., 1995. A Linear Thermohaline Oscillator Driven by Stochastic Atmosphere Forcing. Journal of Climate 8, 2440–2453.

Harper, L. S., Jayne, S. R., St. Laurent, L., Weaver, A. J., 2004. Tidally driven mixing in a numerical model of the ocean general circulation. Ocean Modelling 6, 245–263.

Hasumi, H., Suighinohara, N., 1999. Effects of locally enhanced vertical diffusivity over rough bathymetry on the world ocean circulation. Journal of Geophysical Research 104, 23367–23374.

Hoffert, M. I., Broecker, W. S., 1978. Apparent vertical eddy diffusion reates in the pycnocline of the Norwegian Sea as determined from the vertical distributium of tritium. Geophysical Research Letters 5, 502–504.

Huang, R. X., 1999. Mixing and Energetics of the Oceanic Thermohaline Circulation. Journal of Physical Oceanography 29, 727–746.

Jayne, S. R., St. Laurent, L. C., 2001. Parameterizing tidal dissipation over rough topography. Geophysical Research Letters 28, 811–814.

Kim, S.-J., Stössel, A., 2001. Impact of Subgrid-scale Convection on Global Thermohaline Properties and Circulation. Journal of Physical Oceanography 31, 656–674.

Kim, Y., Eckermann, S. D., Chun, H., 2003. An overview of the past, present and future of gravity drag parameterization for numerical climate and weather prediction models. Atmosphere-Ocean 41, 65–98.

Klinger, B. A., Drijfhout, S., Marotzke, J., Scott, J. R., 2003. Sensitivity of basinwide meridional overturning to diapycnal diffusion and remote wind forcing in an idealized atlantic-southern ocean geometry. Journal of Physical Oceanography 33, 249–266.

Knorr, G., Lohmann, G., 2003. Southern Ocean Origin for Resumption of Atlantic Thermohaline Circulation during Deglaciation. Nature 424, 532–

536.

Levermann, A., Griesel, A., 2004. Solution of a Model for the Oceanic Pycnocline Depth: Scaling of Overturning Strength and Meridional Pressure Difference. Geophysical Research Letters 31, L17302, doi:10.1029/2004GL020678.

Manabe, S., Stouffer, R. J., 1993. Century-scale effects of increased atmospheric CO2 on the ocean-atmosphere system. Nature 364, 215–218.

Manabe, S., Stouffer, R. J., 1999. Are two modes of the thermohaline circulation stable? Tellus A 51, 400–411.

Marotzke, J., Scott, J., 1999. Convective Mixing and the Thermohaline Circulation. Journal of Physical Oceanography 29, 2962–2970.

McManus, J. F., Francois, R., Gherardi, J., Keigwin, L. D., Brown-Leger, S., 2004. Collapse and rapid resumption of Atlantic meridional circulation linked to deglacial climate changes. Nature 428, 834–837.

Mohammad, R., Nilsson, J., 2004. The role of diapycnal mixing for the equilibrium response of thermohaline circulation. Ocean Dynamics 54, 54–65.

Munk, W., Wunsch, C., 1998. Abyssal recipes II: energetics of tidal and wind mixing. Deep-Sea Research Part I 45, 1977–2010.

Nilsson, J., Broström, G., Walin, G., 2003. The Thermohaline Circulation and Vertical Mixing: Does Weaker Density Stratification Give Stronger Overturning? Journal of Physical Oceanography 33, 2781–2795.

Nilsson, J., Walin, G., 2001. Freshwater forcing as a booster of thermohaline circulation. Tellus A 53, 629–641.

OECD, 1985. Review of the continued suitability of the dumping site for radiactive waste in the North-East Atlantic. NEA, OECD, Paris.

Oliver, K. I. C., Watson, A. J., Stevens, D. P., 2005. Can limited ocean mixing buffer rapid climate change? Tellus A 57, 676–690.

Otterå, O. H., Drange, H., Bentsen, M., Kvamstø, N. G., Jiang, D., 2003. The sensitivity of the present-day Atlantic meridional overturning circulation to freshwater forcing. Geophysical Research Letters 30, 1898, doi:10.1029/2003GL017578.

Otterå, O. H., Drange, H., Bentsen, M., Kvamstø, N. G., Jiang, D., 2004. The transient response of the Atlantic Meridional Overturning Circulation to enhanced freshwater input to the Nordic Seas-Arctic Ocean in the Bergen Climate Model. Tellus A 56, 342–361.

Park, Y., 1999. The Stability of Thermohaline Circulation in a Two-Box Model. Journal of Physical Oceanography 29, 3101–3110.

Park, Y., Brian, K., 2000. Comparison of Thermally Driven Circulations from a Depth-Coordinate Model and an Isopycnal-Layer Model. Part I: Scaling-Law Sensitivity to Vertical Diffusivity. Journal of Physical Oceanography 30, 590–605.

Prange, M., Lohmann, G., Paul, A., 2003. Influence of Vertical Mixing on the Thermohaline Hysteresis: Analysis of an OGCM. Journal of Physical Oceanography 33, 1707–1721.

Rahmstorf, S., 1995. Bifurcations of the Atlantic thermohaline circulation in

response to changes in the hydrological cycle. Nature 378, 145–149.
Rahmstorf, S., 2002. Ocean circulation and climate during the past 120,000 years. Nature 419.
Rehmann, C. R., Duda, T. F., 2000. Diapycnal Diffusivity Inferred from Scalar Microstructure Measurements near the New England Shelf/Slope Front. Journal of Physical Oceanography 30, 1354–1371.
Saenko, O. A., Weaver, A. J., 2003. Southern Ocean Upwelling and eddies: sensitivity of the global overturning to the surface density range. Tellus A 55, 106–111.
Sandström, J. W., 1908. Dynamische Versuche mit Meerwasser. Annalen der Hydrographie und der Maritimen Meteorologie 36, 6–23.
Sarmiento, J. L., Feely, H. W., Moore, W. S., Bainbridge, A. E., Broecker, W. S., 1976. The Relationship Between Vertical Eddy Diffusion and Buoyancy Gradient in the Deep Sea. Earth and Planetary Science Letters 32, 357–370.
Schiller, A., Mikolajewicz, U., Voss, R., 1997. The stability of the North Atlantic thermohaline circulation in a coupled ocean-atmosphere general circulation model. Climate Dynamics 13, 325–347.
Schmittner, A., Stocker, T. F., 1999. The Stability of the Thermohaline Circulation in Global Warming Experiments. Journal of Climate 12, 1117–1133.
Simmons, H. L., Jayne, S. R., St. Laurent, L. C., Weaver, A. J., 2004. Tidally driven mixing in a numerical model of the ocean general circulation. Ocean Modelling 6, 245–263.
Stommel, H., 1961. Thermohaline convection with two stable regimes of flow. Tellus 13, 224–230.
Toggweiler, J. R., Samuels, B., 1995. Effect of Drake Passage on the global thermohaline circulation. Deep-Sea Research Part I 42, 477–500.
Tziperman, E., Toggweiler, J. R., Feliks, Y., Bryan, K., 1994. Instability of the Thermohaline Circulation with Respect to Mixed Boundary Conditions: Is It Really a Problem for Realistic Models? Journal of Physical Oceanography 24, 217–232.
Vellinga, M., Wood, R. A., Gregory, J. M., 2002. Processes governing the recovery of a perturbed thermohaline circulation in HadCM3. Journal of Climate 15, 764–780.

List of Figures

List of Tables

2 Properties of the four different regimes for the standard parameter set. The arrows indicate increase (↑) and decrease (↓) of the corresponding properties in response to an increased freshwater flux 20

Parameter	Value
L	12000 km
B	5000 km
D	4000 m
A_i	1000 $m^2\ s^{-1}$
L_y	1500 km
f	$1.5{\cdot}10^{-4}\ s^{-1}$
β	$2{\cdot}10^{-11}\ s^{-1}\ m^{-1}$
ρ_0	1027 $kg\ m^{-3}$
c	$9{\cdot}10^{-5}\ m^2\ s^{-1}$
N_0	$8{\cdot}10^{-3}\ s^{-1}$
C	0.5
τ	0.12 $N\ m^{-2}$
$T_{n_{\mathrm{relax}}} = T_{s_{\mathrm{relax}}}$	3 °C
$T_{e_{\mathrm{relax}}}$	25 °C
$\gamma_n = \gamma_e = \gamma_s$	5 yr
$S_{s_{\mathrm{relax}}}$	34.5 PSU
γ_s^S	100 yr
F_n	0.24 Sv
F_e	-0.4 Sv

Table 1
Standard parameter set used for all experiments, if not mentioned otherwise in the text

		Regime 1	Regime 2	Regime 3	Regime 4
		$0 \le \alpha \le \alpha_{\mathrm{heat}}$	$\alpha_{\mathrm{heat}} < \alpha \le \alpha_{\mathrm{Psi}}$	$\alpha_{\mathrm{psi}} < \alpha \le \alpha_{T_{\mathrm{no}}}$	$\alpha > \alpha_{T_{\mathrm{no}}}$
Response to	Ψ_{No}	↓	↓	↑	↑
increased F_n	Heat flux	↓	↑	↑	↑
	T_n	↓	↓	↓	↑

Table 2
Properties of the four different regimes for the standard parameter set. The arrows indicate increase (↑) and decrease (↓) of the corresponding properties in response to an increased freshwater flux

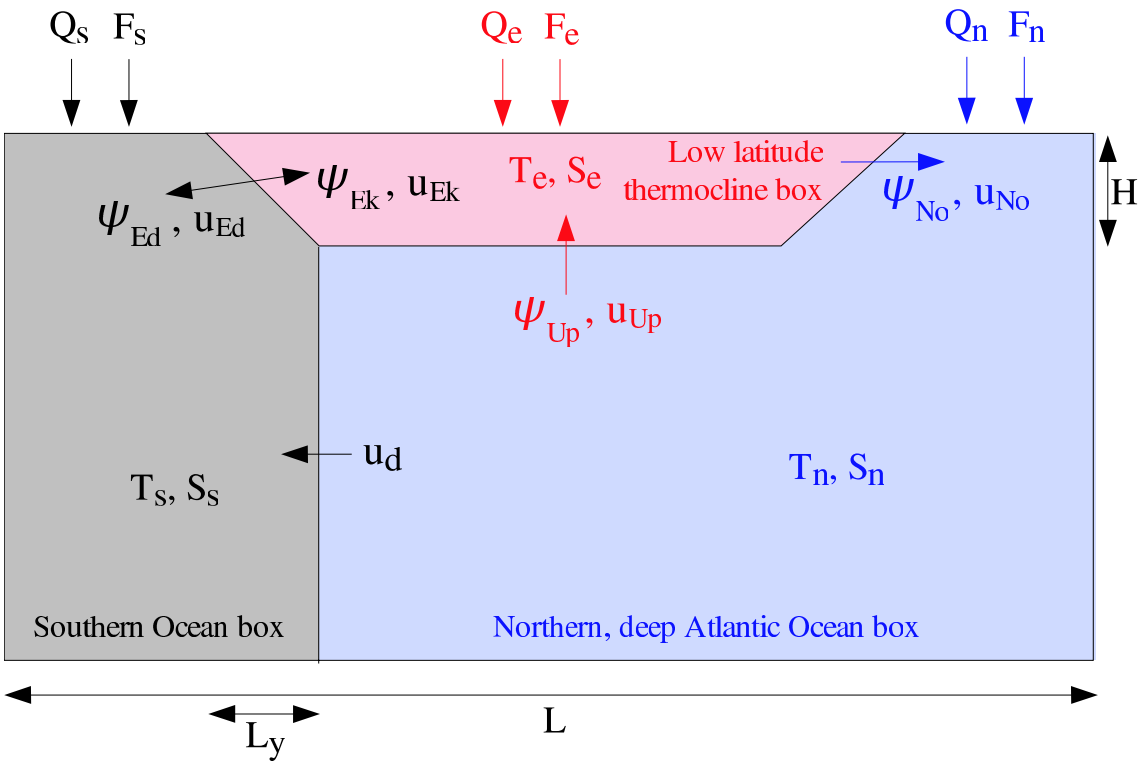

Fig. 1. Schematic representation of the model

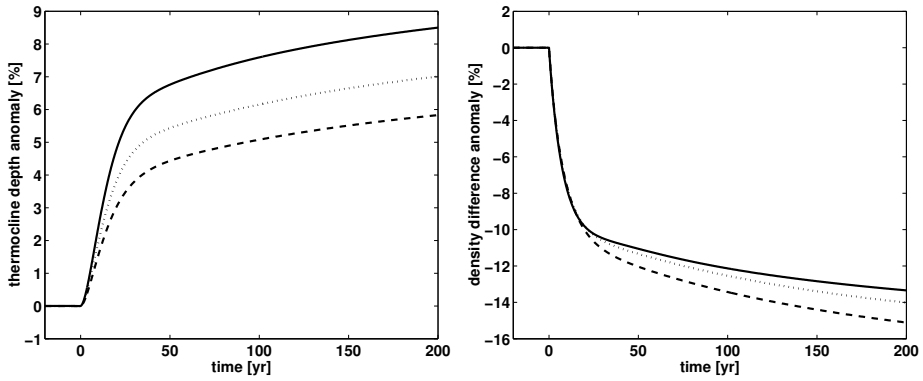

Fig. 2. Left: anomaly of the thermocline depth after the freshwater flux is increased by 50% at $t = 0$. Dashed line $\alpha = 0$, dotted line $\alpha = 0.5$, solid line $\alpha = 1$. Right: anomaly of the density difference between the thermocline and northern boxes.

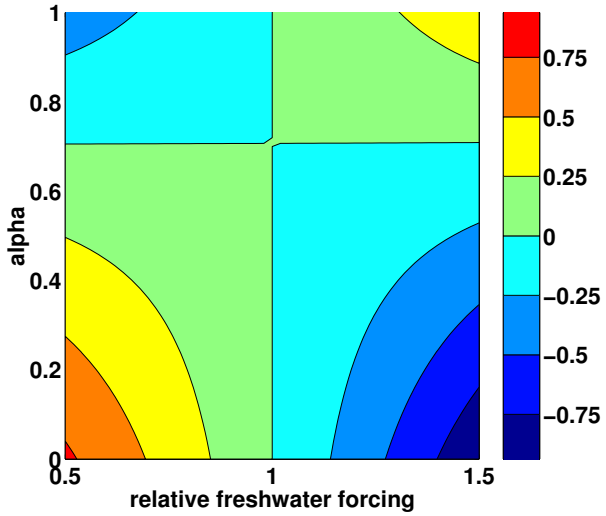

Fig. 3. Anomaly of the northward volume transport Ψ_{No} [Sv] as a function of the relative freshwater forcing F_n, and α. $F_n = 1$ corresponds to the default value of 0.24 Sv, the zero anomaly contour corresponds to 18 Sv of overturning.

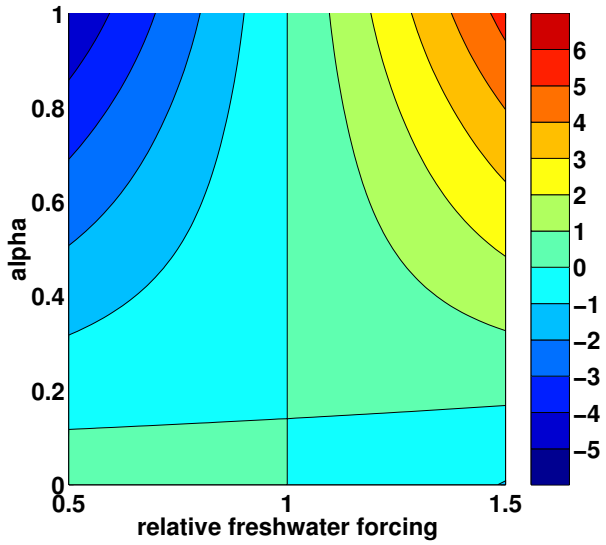

Fig. 4. As fig. 3, but for the anomaly of the northward effective heat transport [%]. The zero anomaly contour corresponds to ~ 1.2 PW heat transport in the model.

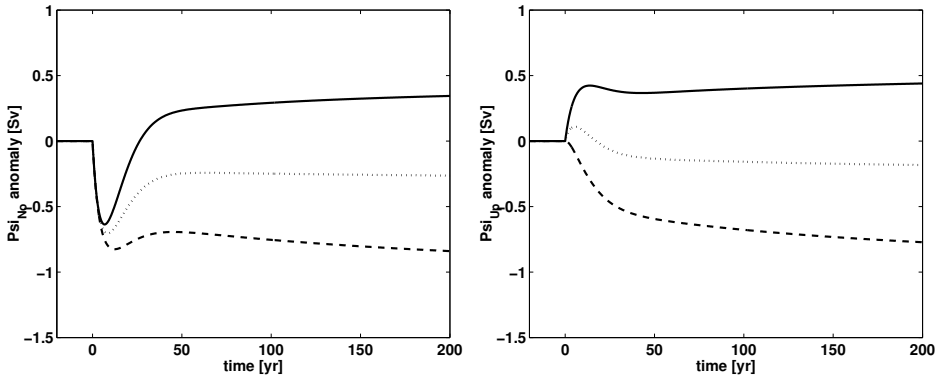

Fig. 5. As figure 2, but left: anomalous northward volume transport. Right: upwelling into the thermocline box.

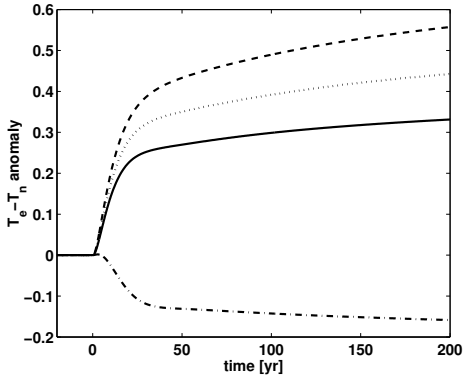

Fig. 6. Anomaly of the temperature difference between low latitudes and northern box. Dashed, dotted, solid as in figures 2 and 5, dash-dotted for $\alpha = 3$

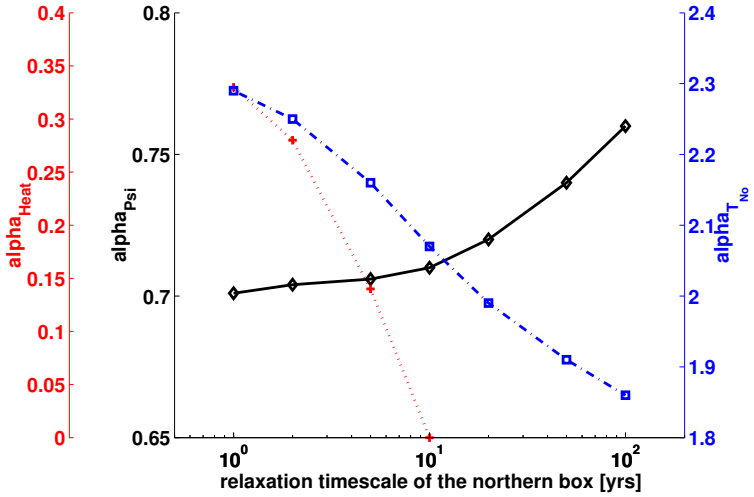

Fig. 7. Dependency of the critical values of α on the timescale of temperature relaxation in the northern box. Dotted line: α_{Heat}, dash-dotted line: $\alpha_{T_{\mathrm{No}}}$, solid line: α_{Psi}

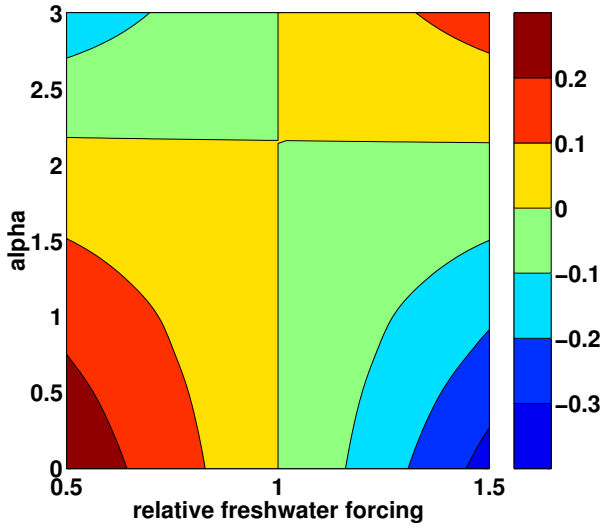

Fig. 8. Anomaly of temperature of the northern and deep box T_n [K] as a function of F_n and α (note that the scale for α is different from the previous plots)

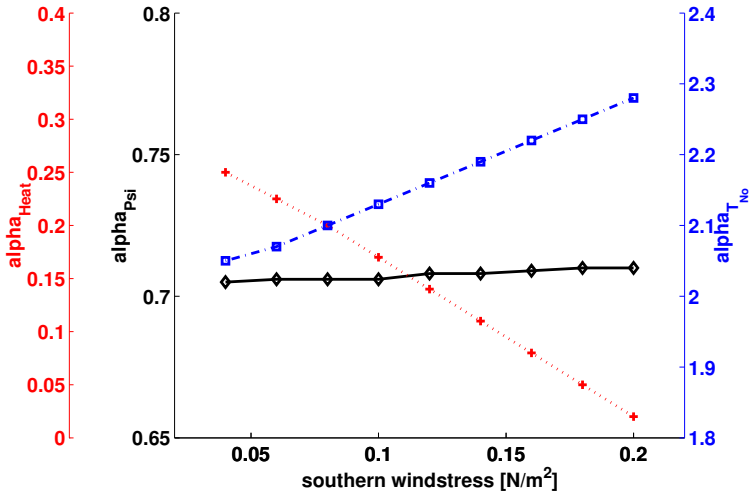

Fig. 9. Dependency of the critical values of α on the strength of southern ocean wind forcing. Lines as in fig. 7